Probabilistic Engineering Mechanics 79 (2025) 103735

Contents lists available at ScienceDirect

Probabilistic Engineering Mechanics

journal homepage: www.elsevier.com/locate/probengmech

Stochastic dynamic response analysis via dimension-reduced probability density evolution equation (DR-PDEE) with enhanced tail-accuracy

Yi Luo [a,b], Chao Dang [c,*], Matteo Broggi [a], Michael Beer [a,d,e]

[a] Institute for Risk and Reliability, Leibniz University Hannover, Callinstraße 34, Hannover, 30167, Germany
[b] Department of Civil and Environmental Engineering, Rice University, 6100 Main Street, Houston, 77005, TX, USA
[c] Chair for Reliability Engineering, TU Dortmund Univeristy, Leonhard-Euler-Str. 5, Dortmund, 44227, Germany
[d] Department of Civil and Environmental Engineering, University of Liverpool, Liverpool, L69 3GH, UK
[e] International Joint Research Center for Resilient Infrastructure & International Joint Research Center for Engineering Reliability and Stochastic Mechanics, Tongji University, Shanghai, 200092, China

ARTICLE INFO

Keywords:
Dimension-reduced probability density evolution equation (DR-PDEE)
Tail accuracy
Stochastic response analysis
Multi-dimensional nonlinear systems

ABSTRACT

The stochastic dynamic analysis of high-dimensional nonlinear systems is a critical concern in engineering fields, especially when considering the reliability analysis of low-probability events. To address this challenge, the dimension-reduced probability density evolution equation (DR-PDEE) method has recently emerged as a promising tool. The DR-PDEE is the analytical governing equation for the probability density function (PDF) evolution of any path-continuous stochastic process. For a single response quantity of interest in a multi-dimensional nonlinear dynamic system, the corresponding DR-PDEE is merely a one- or two-dimensional partial differential equation. After estimating the intrinsic drift coefficient (IDC) in the DR-PDEE from sample data, this equation can be easily solved with rather high accuracy. However, if only a limited number of deterministic analyses are affordable, there is usually no sample information for the tail estimation of the IDC, resulting in an inaccurate PDF solution in the tail. In this work, a scheme is tailored for the DR-PDEE to further enhance its tail accuracy. Specifically, to increase the occurrence probability of tail samples, an additional set of samples is obtained by simply magnifying the excitation intensity of the system. Then, at each time step, samples in the response tail from this additional set are identified. By merging these samples with samples from the original system, a better IDC estimation in the tail is achieved. Several numerical examples are investigated to validate the effectiveness of the proposed DR-PDEE method. Comparisons with MCS and the classical DR-PDEE method show that the proposed scheme improves the accuracy and robustness of the PDF results in the tail.

1. Introduction

Real-world engineering systems are always subject to various sources of randomness, either from random parameters or from stochastic excitations [1–3]. To understand their behavior and reliability, the stochastic dynamic analysis of high-dimensional nonlinear systems becomes a critical topic in scientific and engineering communities. Especially when analyzing reliability, an accurate and robust estimation of the response statistics in the low-probability range is of significant importance. Since the 1950s, the study of stochastic dynamic systems has been extensively explored, leading to the development of numerous methods, which can be briefly categorized as sample-based and non-sample-based methods.

In the realm of non-sample-based methods, addressing different sources of randomness has resulted in two primary directions. First, for problems involving randomness stemming solely from system parameters, methods such as random perturbation [4], stochastic collocation [5,6], and polynomial chaos expansion [7] have been extensively investigated. However, since these methods usually involve a further extension of the dimensions of the original system, they often suffer from the so-called curse of dimensionality.

Second, the field of random vibration theory has emerged to tackle the nonlinear systems subjected to stochastic excitations, yielding a series of governing equations of the probability density function (PDF) [8].

This article is part of a special issue entitled: Stochastic Mechanics EMI 2023 published in Probabilistic Engineering Mechanics.

* Corresponding author.
E-mail addresses: yi.luo@irz.uni-hannover.de (Y. Luo), chao.dang@tu-dortmund.de (C. Dang), broggi@irz.uni-hannover.de (M. Broggi), beer@irz.uni-hannover.de (M. Beer).

https://doi.org/10.1016/j.probengmech.2025.103735
Received 30 August 2024; Received in revised form 21 December 2024; Accepted 23 January 2025
Available online 25 January 2025

Among these, the Fokker–Planck–Kolmogorov (FPK) equation stands out as one of the most extensively studied equations. Analytical solutions for the FPK equation are limited to specific systems [9–11], while numerical solutions are typically obtained through methods such as finite element [12], finite difference [13], and path integration [14]. For higher-dimensional systems, dimension reduction techniques have been developed to obtain approximate solutions, including the stochastic averaging method [15,16] and state-space-split method [17]. Yet, these methods are constrained by the Markovian assumption and struggle to effectively extend to complex engineering problems. Another category of approaches involves approximating results at the moment level, such as statistical linearization [1] and moment closure [18,19]. However, these approaches rely on the truncation of response moments, making it difficult to precisely characterize the PDF for strongly nonlinear problems.

The sample-based method mainly refers to the Monte Carlo technique and its variance reduction versions. Specifically, stratified and Latin hypercube sampling schemes [20,21], as well as many deterministic low-discrepancy point sets [22,23] have been developed to improve the accuracy and robustness of Monte Carlo simulation. For PDF estimation, methods include direct calculation based on sample frequencies, kernel smoothing techniques, and distribution fitting methods such as the maximum entropy and fractional-order moment method [24–27]. However, these approaches may struggle to capture probability tails accurately. Specifically, for reliability analysis of low-probability events, advanced Monte Carlo methods such as subset simulation [28,29], importance sampling [30,31], line sampling ([32], Dang et al. [33,34]), and directional sampling [35,36] have been developed. To further enhance sample utilization, sequential sampling, adaptive sampling, and surrogate models have been extensively investigated [37–39]. However, the high-dimensional nature of many engineering systems, the multiple correlative variables involved, and their complex interactions significantly magnify the difficulty of devising an efficient sampling strategy [40]. Despite the progress in advanced Monte Carlo techniques, achieving accurate and computationally feasible tail estimations of probability distributions for stochastic dynamic engineering systems remains a persistent challenge.

Instead of directly capturing the probability information from samples as in Monte Carlo Simulation, the recently developed dimension-reduced probability density evolution equation (DR-PDEE) provides a new perspective for the stochastic dynamic response analysis [41,42]. Specifically, in the DR-PDEE method, the problem of PDF determination is divided into two parts. First, establish the equation governing the transient PDF of the response process of interest, namely the DR-PDEE; second, determine the intrinsic drift coefficient (IDC) in the equation.

The first part, namely the establishment of the DR-PDEE, is the theoretical foundation. It originated from explorations into the equivalence of probability density evolution method (PDEM) [43,44] and dimension-reduced Fokker-Planck-Kolmogorov (DR-FPK) equations [45–48]. However, it wasn't until the past two years, with the extension to general path-continuous stochastic processes via Kramers-Moyal expansion [41,42], that the DR-PDEE emerged as a new equation with remarkable vitality. This development greatly expands its applicability, overcoming the Markovian limitations of DR-FPK equations and unifying the treatment of system parameters and excitation randomness [42]. Furthermore, the DR-PDEE fundamentally overcomes the curse of dimensionality. On the one hand, adopting a state-space description frees the DR-PDEE from constraints related to the dimensionality and correlations of system random variables. On the other hand, for an arbitrarily-high-dimensional dynamic system, the DR-PDEE is always a one- or two-dimensional partial differential equation solely involving the response quantities of interests, facilitating the convenient solution of the response PDFs. These advantages are evident in its successful applications to the stochastic dynamic response analysis (Luo et al. [34, 42,49,50]) and first-passage reliability analysis [41,51,52] of high-dimensional complex dynamic systems.

Correspondingly, the second part, estimating the IDC, is pivotal for the numerical implementation of the DR-PDEE method. Given that analytical solutions for IDC are only attainable for a few nonlinear systems [53], numerical estimation is generally achieved through sampling [42,50]. Fortunately, the nature of IDC as a conditional expectation allows for a significantly reduced sample size compared to direct PDF estimation. Thisrepresents an intrinsic advantage over traditional Monte Carlo methods. However, when only a limited sample computations are feasible, almost no samples will fall into the tail range. In such cases, estimating IDC in the tail range relies on extrapolation. This will lead to deviations and low robustness in the tail estimation of the IDC, and subsequently result in low accuracy in the PDF tail.

This study proposes a simple and practical strategy for the DR-PDEE method to further enhance its tail accuracy. Specifically, by amplifying the excitation intensity of the original system, an additional set of samples with higher probability of falling in the response tail is obtained. At each computational time step, samples in the tail range from this set are identified and combined with another set of samples obtained from the original system to estimate the IDC. The rationality of the scheme is explained from the perspective of importance sampling. Several numerical examples are studied to validate the effectiveness of the proposed approach. These include a multi-dimensional linear system, a single-degree-of-freedom (SDOF) nonlinear oscillator, a two-degrees-of -freedom (DOF) vibro-impact oscillator, and a ten-DOF Duffing oscillator with random parameters. Additionally, in Appendix, a specific class of nonlinear cases whose IDCs are independent of excitation intensity is provided.

This paper is organized as follows. Section 2 provides the fundamentals of the DR-PDEE. Section 3 introduces the proposed tail-enhanced DR-PDEE scheme in detail. Section 4 presents the numerical examples. Section 5 dicusses the conclusions and possible further improvements.

2. Dimension-reduced probability density evolution equation

2.1. Theoretical formulation

This section serves as a brief background on the dimension-reduced probability density evolution equation (DR-PDEE). More details can be found in references [41,42].

As mentioned previously, the DR-PDEE is the governing equation for the transient PDF of any path-continuous stochastic process. For simplicity, consider a one-dimensional stochastic process $Y(t)$. Its probability density function (PDF) at time $t = t' + \Delta t$ $(t' < t)$ can be given by the PDF at time t' and the conditional PDF $p(y,t|y',t')$, that is,

$$p(y,t) = \int_{-\infty}^{+\infty} p(y,t|y',t')p(y',t')\mathrm{d}y' \tag{1}$$

Converting the above integral equation into differential form yields the well-known Kramers-Moyal expansion [54–56]

$$\frac{\partial p(y,t)}{\partial t} = \sum_{n=1}^{\infty} \frac{(-1)^n}{n!} \frac{\partial^n}{\partial y^n}[\alpha_n(y,t)p(y,t)] \tag{2}$$

where

$$\alpha_n(y,t) = \lim_{\Delta t \to 0} \mathrm{E}[\Delta Y^n(t) / \Delta t | Y(t) = y], \text{for } n = 1, 2, \cdots \tag{3}$$

is the $n-$ th order conditional derivative moment.

Further, the process $Y(t)$ is constrained to be path-continuous by addressing the condition [8] that for any $\varepsilon > 0$,

$$\lim_{\Delta t \to 0} \frac{1}{\Delta t} \int_{|y-y'|>\varepsilon} p(y,t|y',t')\mathrm{d}y = 0 \tag{4}$$

If Eq. (4) is satisfied, then the path of $Y(t)$ is a continuous function in time with probability one. This means that for any arbitrary $\varepsilon > 0$, the

integrand in Eq. (4) should be zero almost everywhere. Consequently, for any $n \geq 3$ and $\varepsilon > 0$, one has [41]

$$\begin{aligned}|\alpha_n(y,t)| &= \lim_{\Delta t\to 0}\frac{1}{\Delta t}\int_{-\infty}^{\infty}|\xi|^n p(y+\xi,t+\Delta t|y,t)\mathrm{d}\xi \\ &= \lim_{\Delta t\to 0}\frac{1}{\Delta t}\int_{-\varepsilon}^{\varepsilon}|\xi|^n p(y+\xi,t+\Delta t|y,t)\mathrm{d}\xi \\ &= \lim_{\Delta t\to 0}\frac{1}{\Delta t}\int_{-\varepsilon}^{\varepsilon}|\xi|^{n-2}\xi^2 p(y+\xi,t+\Delta t|y,t)\mathrm{d}\xi \\ &\leq \varepsilon^{n-2}\lim_{\Delta t\to 0}\frac{1}{\Delta t}\int_{-\varepsilon}^{\varepsilon}\xi^2 p(y+\xi,t+\Delta t|y,t)\mathrm{d}\xi.\end{aligned} \tag{5}$$

In Eq. (5), the last term is $\varepsilon^{n-2}\alpha_2(y,t)$. Due to the arbitrariness of ε, one has $\alpha_n(y,t) = 0$ for $n \geq 3$.

Therefore, for a path-continuous process, only the first two terms are left in the Kramers-Moyal expansion [Eq. (2)]. By denoting the first and second order conditional derivative moments as the intrinsic drift coefficient $a^{(\mathrm{int})}(y,t) = a_1(y,t)$, and the intrinsic diffusion coefficient $b^{(\mathrm{int})}(y,t) = a_2(y,t)$ respectively, it yields

$$\frac{\partial p(y,t)}{\partial t} = -\frac{\partial[a^{(\mathrm{int})}(y,t)p(y,t)]}{\partial y} + \frac{1}{2}\frac{\partial^2\left[b^{(\mathrm{int})}(y,t)p(y,t)\right]}{\partial y^2} \tag{6}$$

Eq. (6) is just the DR-PDEE for generic path-continuous processes. For a stochastic process of higher dimension, its DR-PDEE can also be established similarly.

Consider a response-continuous $m-$ dimensional dynamic system subject to random system parameters and stochastic excitation. Its state equation can be given by

$$\dot{\boldsymbol{X}}(t) = \boldsymbol{G}(\boldsymbol{X}(t),\boldsymbol{\Theta}) + \boldsymbol{f}(t) \tag{7}$$

where $\boldsymbol{X}(t)$ and $\dot{\boldsymbol{X}}(t)$ denote the $m-$ dimensional response and its time-derivative, respectively; $\boldsymbol{\Theta} = [\Theta_1, \Theta_2, \cdots, \Theta_s]^{\mathrm{T}}$ is an $s-$ dimensional random vector; $\boldsymbol{G}(\cdot)$ is an $m-$ dimensional deterministic function; and $\boldsymbol{f}(t)$ is an $m-$ dimensional stochastic excitation.

If only the $l-$ th dimension of the response is of interest, namely $Y(t) = X_l(t)$, its corresponding DR-PDEE is given by Eq. (6), and the intrinsic drift coefficient can be given by

$$a^{(\mathrm{int})}(y,t) = \mathrm{E}[\dot{Y}(t)|Y(t) = y] \tag{8}$$

Furthermore, for the majority of multi-dimensional nonlinear systems, the closed-form solution of $a^{(\mathrm{int})}(y,t)$ is not available.

As for the intrinsic diffusion coefficients, if the $l-$ th component of $\boldsymbol{f}(t)$ is Gaussian white noise that satisfies

$$\mathrm{E}[f_l(t)] = 0, \mathrm{E}[f_l(t)f_l(t+\tau)] = D(t)\delta(\tau) \tag{9}$$

it follows that

$$b^{(\mathrm{int})}(y,t) = D(t) \tag{10}$$

Otherwise,

$$b^{(\mathrm{int})}(y,t) = 0 \tag{11}$$

Therefore, the intrinsic diffusion coefficients can be determined analytically.

2.2. Implementation of the DR-PDEE

In the previous section, the DR-PDEE, as well as the intrinsic diffusion coefficient $b^{(\mathrm{int})}(y,t)$, has been established analytically. However, the DR-PDEE remains unclosed due to the unresolved intrinsic drift coefficient (IDC) $a^{(\mathrm{int})}(y,t)$. Consequently, the procedure of solving the response PDF via the DR-PDEE involves two steps: first, estimating the IDC, and second, solving the DR-PDEE. These two steps also introduce potential sources of error in the DR-PDEE approach.

It is paramount to understand that the error introduced from solving the DR-PDEE is reducible. As indicated earlier, when the excitation $f_l(t)$ is not Gaussian white noise, the intrinsic diffusion coefficient $b^{(\mathrm{int})}(y,t)$ is zero. Consequently, the DR-PDEE transforms into a hyperbolic partial differential equation. When tail accuracy is critical, the numerical error in solving such equations becomes non-trivial [2]. To circumvent this issue for systems subject to non-white noise excitation, it is suggested to simulate the excitation as filtered white noise using a prefilter, and then integrate the filter equation into the original equation of motion to construct an augmented system [49]. Subsequently, an analytically known non-zero diffusion coefficients is introduced. Then, the DR-PDEE can be solved with sufficiently high accuracy via numerical path integration.

Furthermore, the estimation of the intrinsic drift coefficients $a^{(\mathrm{int})}(y,t)$ is considered. Eq. (8) can be rewritten as

$$a^{(\mathrm{int})}(y,t) = \mathrm{E}[G_l(\boldsymbol{X}(t),\boldsymbol{\Theta})|X_l(t) = Y(t) = y] \tag{12}$$

If no analytical solution is available, a common approach is to estimate $a^{(\mathrm{int})}(y,t)$ from the samples of $X_l(t)$ and of $G_l(\boldsymbol{X}(t),\boldsymbol{\Theta})$. Numerical techniques such as the locally weighted smoothing scatterplots (LoWeSS) [57] and the vine-copula-based estimator [42] have been proven effective.

Based on the above discussion, the estimation of $a^{(\mathrm{int})}(y,t)$ is the key aspect of ensuring the accuracy of the DR-PDEE solution. Generally speaking, the more exact-analytical information of $a^{(\mathrm{int})}(y,t)$ that is known, the higher level of accuracy that can be achieved in the estimation process. Therefore, if some prior knowledge regarding the functional form of $a^{(\mathrm{int})}(y,t)$ is accessible, parametric regression methods such as least squares regression are preferred. However, for complex systems in real-world engineering subject to multiple sources of randomness, the form of $a^{(\mathrm{int})}(y,t)$ is usually unavailable. Meanwhile, only a limited number of deterministic analyses can be affordable. Consequently, with no sample information in the tail, the tail estimation of $a^{(\mathrm{int})}(y,t)$ purely relies on extrapolation. This would lead to unpredictable and, most probably, significant errors in the tail estimation, as illustrated by Fig. 1.

3. Data-assisted DR-PDEE with enhanced tail accuracy

3.1. Challenges

As discussed in the previous section, the primary limitation of the data-assisted DR-PDEE method is the lack of sample information in the

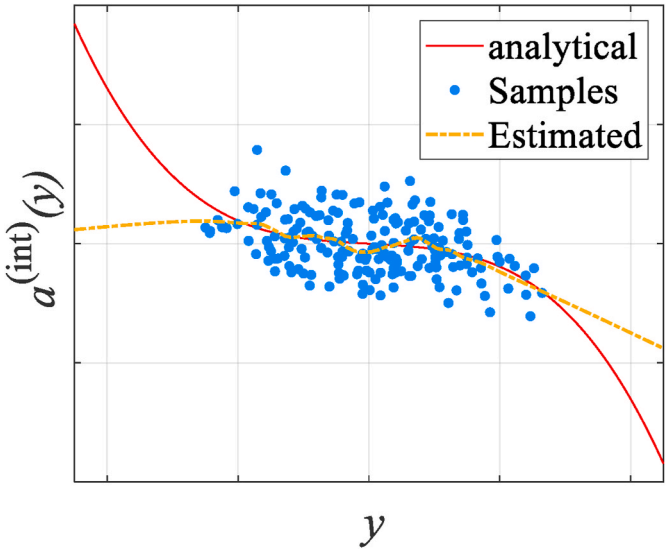

Fig. 1. Schematic of numerical estimation of $a^{(\mathrm{int})}(y,t)$ using direct Monte Carlo samples.

tail range. Therefore, acquiring samples in the tail is crucial for enhancing the tail accuracy of the method. However, the procedure of stochastic dynamic response analysis via DR-PDEE introduces additional challenges to this task.

The first challenge is the exceedingly high dimension of random parameters involved. To guarantee tail accuracy in solving the DR-PDEE, the stochastic excitation of the system is always considered as, or transferred into, Gaussian white noise. Consequently, the dimension of the random parameters involved should be theoretically infinite. Even with a discrete time interpretation, the random parameters are still of extremely high dimension, because at least one new random variable is introduced at every time increment. Moreover, the random variables introduced from the Gaussian white noise are independent and identically distributed. This means these dimensions are equally important, and thus dimension reduction schemes can hardly be applied.

The second difficulty is unique for the stochastic response analysis via DR-PDEE. In the current numerical procedure, the intrinsic drift coefficients need to be estimated separately at every time step. This is particularly crucial in cases of non-stationary excitation when time-varying response statistics are important. However, due to the stochastic oscillating nature of the samples, those falling in the tail region always vary at different time instances. Consequently, it is difficult to establish a criterion, as in adaptive sampling schemes, to determine which sample is preferred. It should be noted that this issue does not arise in first-passage reliability analyses, where only the extreme value of the entire response process matters.

Given the aforementioned reasons, most of the established adaptive sampling techniques become infeasible for the problem considered in this work. Therefore, a tailored scheme needs to be devised specifically for the DR-PDEE approach.

3.2. Initial conceptualization: amplifying excitation

In this section, a scheme to further enhance the tail accuracy of the DR-PDEE method is proposed. The main concept of this development centers around directly obtaining samples by amplifying the system's excitation. This scheme stems from a straightforward concept: for the majority of dynamic systems, higher excitation intensity corresponds to larger response amplitudes, thereby increasing the likelihood of obtaining samples in the tail.

However, what is the impact of directly amplifying the excitation intensity on the intrinsic drift coefficient (IDC), or more specifically, on the tail of the IDC? This issue can be analyzed from two perspectives. First, from the standpoint of physical systems, one can obtain analytical insights into the IDC. This enables an assessment of how variations in excitation intensity affect the analytical form of IDC. However, since analytical solutions are available for only a very few systems, it is challenging to generalize the conclusions obtained from this perspective to general systems. The other perspective focuses on the sample space, where the impact of amplifying excitation intensity on the probability measure of input randomness can be examined. This allows for an analysis of how these changes influence the estimation of IDC based on the samples for general systems. The following discussion will explore these two perspectives in detail.

3.2.1. Physical/analytical perspective

Amplifying the excitation intensity of the system leads to a new system, hereafter referred to as the amplified system for simplicity. If the system is linear and involves no random system parameters, it can be easily proved that the IDC of the amplified system and the original system are the same. For any of such systems, it is already known that its IDC is a linear function [58,59]. That is,

$$a^{(\mathrm{int})}(\boldsymbol{y},t)=\mathrm{E}[\dot{\boldsymbol{Y}}(t)|\boldsymbol{Y}(t)=\boldsymbol{y}]=\boldsymbol{k}(t)\boldsymbol{y} \tag{13}$$

If the intensity of the excitation is amplified α times, then the response is also amplified by α. Denote the response of the amplified system as $\overline{\boldsymbol{Y}}(t)$. There is

$$\begin{aligned}\overline{a}^{(\mathrm{int})}(\boldsymbol{y},t)&=\mathrm{E}[\dot{\overline{\boldsymbol{Y}}}(t)|\overline{\boldsymbol{Y}}(t)=\boldsymbol{y}]=\mathrm{E}\left[\alpha\dot{\boldsymbol{Y}}(t)|\boldsymbol{Y}(t)=\frac{1}{\alpha}\boldsymbol{y}\right]=\alpha\boldsymbol{k}(t)\frac{\boldsymbol{y}}{\alpha}\\&=\boldsymbol{k}(t)\boldsymbol{y}=a^{(\mathrm{int})}(\boldsymbol{y},t)\end{aligned} \tag{14}$$

If the system is nonlinear, there are also a few special cases, whose IDCs remain identical before and after amplifying the excitation intensity, including but not limited to the special category of energy equipartition system given in the Appendix, and the vibro-impact oscillator given in the third numerical example.

However, for most linear systems with random parameters, as well as nonlinear systems, the IDCs typically change with the white noise intensity. This is evident in the second numerical example, where an analytical solution for the IDC is available. The analytical solution clearly involves the excitation intensity in its expression, and therefore the IDC varies with change in excitation intensity. Nevertheless, it is also observed that the IDCs corresponding to different excitation intensities converge in the tail. Although currently it is not possible to analytically prove this conclusion for more general systems due to the lack of analytical solutions, no system has yet been found where the available analytical solution contradicts this conclusion. This suggests the feasibility of estimating the tail of IDC using samples from the amplified system.

3.2.2. Sample space perspective

It is possible togain general insights on the influence of amplifying excitation intensity from the sample estimation perspective, and the concept of importance sampling can be employed.

For clarity, assume only one dimension of the system $X_l(t)$ is of concern. Its corresponding drift is denoted as $G_l(t)$. For the considered system, the value of its responses is completely determined by the value of all random sources involved, denoted by random parameters $\boldsymbol{\Theta}$. For a given value of $\boldsymbol{\Theta}=\boldsymbol{\theta}$, the value of $X_l(t)$ and $G_l(t)$ will be accordingly given by deterministic functions as $x_l=H_{x_l}(\boldsymbol{\theta},t)$, and $g_l=H_{g_l}(\boldsymbol{\theta},t)$. For simplicity, t will be omitted later. Then, the IDCcan be given as

$$\begin{aligned}\mathrm{E}(G_l|X_l=x_l)&=\int g_l p(g_l|x_l)\mathrm{d}g_l=\int g_l\frac{p(g_l,x_l)}{p(x_l)}\mathrm{d}g_l\\&=\int g_l\frac{\int p(g_l,x_l,\boldsymbol{\theta})\mathrm{d}\boldsymbol{\theta}}{\int p(x_l,\boldsymbol{\theta})\mathrm{d}\boldsymbol{\theta}}\mathrm{d}g_l\\&=\int g_l\frac{\int\delta\left[x_l-H_{x_l}(\boldsymbol{\theta})\right]\delta\left[g_l-H_{g_l}(\boldsymbol{\theta})\right]p_\Theta(\boldsymbol{\theta})\mathrm{d}\boldsymbol{\theta}}{\int\delta\left[x_l-H_{x_l}(\boldsymbol{\theta})\right]p_\Theta(\boldsymbol{\theta})\mathrm{d}\boldsymbol{\theta}}\mathrm{d}g_l\\&=\frac{\int\delta\left[x_l-H_{x_l}(\boldsymbol{\theta})\right]H_{g_l}(\boldsymbol{\theta})p_\Theta(\boldsymbol{\theta})\mathrm{d}\boldsymbol{\theta}}{\int\delta\left[x_l-H_{x_l}(\boldsymbol{\theta})\right]p_\Theta(\boldsymbol{\theta})\mathrm{d}\boldsymbol{\theta}}\\&=\frac{\int p(x_l,\boldsymbol{\theta})H_{g_l}(\boldsymbol{\theta})\mathrm{d}\boldsymbol{\theta}}{\int p(x_l,\boldsymbol{\theta})\mathrm{d}\boldsymbol{\theta}}\end{aligned} \tag{15}$$

Eq. (15) is an analytical equation. However, theIDC cannot be directly calculated using Eq. (15), and it is usually estimated from samples. Using Monte Carlo samples, the estimation can be given as

$$\mathrm{E}(G_l|X_l=x_l)=\frac{\int p(x_l,\boldsymbol{\theta})H_{g_l}(\boldsymbol{\theta})\mathrm{d}\boldsymbol{\theta}}{\int p(x_l,\boldsymbol{\theta})\mathrm{d}\boldsymbol{\theta}}=\frac{\sum_{q=1}^{N}p^{(q)}(x_l)\cdot g_l^{(q)}}{\sum_{q=1}^{N}p^{(q)}(x_l)} \tag{16}$$

where N is the number of samples, $p^{(q)}(\cdot)$ is the approximated weighting function of sample $\boldsymbol{\theta}^{(q)}$. Notice that $p^{(q)}(x_l)$ analytically involves a Dirac-delta function, i.e. $\int_{\boldsymbol{\Omega}^{(q)}}\delta\left[x_l-H_{x_l}(\boldsymbol{\theta})\right]p_\Theta(\boldsymbol{\theta})\mathrm{d}\boldsymbol{\theta}$, where $\boldsymbol{\Omega}^{(q)}$ is the associated probability space of $\boldsymbol{\theta}^{(q)}$. This means analytically, $p^{(q)}(x_l)$ is extremely localized. However, in numerical estimation schemes, the form of $p^{(q)}(x_l)$ is given empirically with some relaxation.

For the samples from the amplified system, the distributions of the excitation-related random parameters are changed. According to the importance sampling concept, the estimation of theIDC should be given

as

$$\mathrm{E}(G_l|X_l=x_l)=\frac{\sum_{q=1}^{N} p^{(q)}(x_l)\frac{p_0^{(q)}(\boldsymbol{\theta})}{\widetilde{p}^{(q)}(\boldsymbol{\theta})}\cdot g_l^{(q)}}{\sum_{q=1}^{N} p^{(q)}(x_l)\frac{p_0^{(q)}(\boldsymbol{\theta})}{\widetilde{p}^{(q)}(\boldsymbol{\theta})}} \tag{17}$$

where $p_0^{(q)}(\boldsymbol{\theta})$ and $\widetilde{p}^{(q)}(\boldsymbol{\theta})$ are respectively the probability density at $\boldsymbol{\theta}^{(q)}$ with respect to the stochastic excitation of the original system and the amplified system.

Notice that the excitation is Gaussian white noise, and is analytically infinite dimensional. The computation of the ratio $p_0^{(q)}(\boldsymbol{\theta})/\widetilde{p}^{(q)}(\boldsymbol{\theta})$ is very tricky. A polar coordinate transformation may facilitate the computation. An $n-$ dimensional independent standard normal vector $\boldsymbol{U}$ can be transferred into $\boldsymbol{U}=R\boldsymbol{A}$, where $R=\|\boldsymbol{U}\|$ is the radius, $\boldsymbol{A}=\boldsymbol{U}/\|\boldsymbol{U}\|$ is the random directional unit vector. R and $\boldsymbol{A}$ are independent [60]. $\boldsymbol{A}$ is uniformly distributed on a $(n-1)$-dimensional unit hypersphere, with the joint PDF given as

$$f_{\boldsymbol{A}}(\boldsymbol{a})=\frac{\Gamma(n/2)}{2\pi^{n/2}} \tag{18}$$

where $\Gamma(\cdot)$ is the Gamma function. Since the sum of the squares of n independent standard normal random variables follows a chi-square distribution with n degrees of freedom, the distribution of R is given by a so-called "chi distribution" expressed as

$$f_R(r)=\frac{2\exp(-r^2/2)r^{n-1}}{2^{n/2}\Gamma(n/2)} \tag{19}$$

As the dimension n tends to infinity, the distribution of R becomes a normal distribution with mean of $\sqrt{n}$ and variance of 0.5 [61].

Then, consider the stationary Gaussian white noise input in a discretized form. At each time step, a new normal distributed increment $\mathrm{d}W$ will be introduced with zero mean and variance of $D\mathrm{d}t$, where D is the white noise intensity. Then, the mean and variance of radius for the input normal vector $\boldsymbol{\theta}$ can be derived as

$$\mu_R=\lim_{\substack{n\to\infty\\ \mathrm{d}t\to 0}}\sqrt{D\mathrm{d}t\cdot n}=\mathrm{E}\left[\int_0^T(\mathrm{d}W)^2\right]=DT \tag{20}$$

and

$$\sigma_R^2=\lim_{\substack{n\to\infty\\ \mathrm{d}t\to 0}}(D\mathrm{d}t)\times 0.5=0 \tag{21}$$

This means, for Gaussian white noise excitation input, the radius is analytically a deterministic constant DT. By altering the input intensity by a factor α, no change will be made on the directional vector $\boldsymbol{A}$, but the radius changes into αDT. Consequently, the ratio $p_0^{(q)}(\boldsymbol{\theta})/\widetilde{p}^{(q)}(\boldsymbol{\theta})$ becomes zero for all the samples from the amplified system.

However, the estimation of conditional mean given by Eq. (17) is based on the local relative weight, namely, $p^{(q)}(x_l)\frac{p_0^{(q)}(\boldsymbol{\theta})}{\widetilde{p}^{(q)}(\boldsymbol{\theta})}$, of each sample. Supposing one has obtained some samples from both the amplified system and the original system. For samples that fall within the peak region and therefore mixed with the samples from the original system, the importance ratio $p_0^{(q)}(\boldsymbol{\theta})/\widetilde{p}^{(q)}(\boldsymbol{\theta})$ should be zero. Whereas, in the tail region, only samples from the amplified systems can be found. Then, for all these samples, their original PDF function value can be considered equal, i.e.

$$\frac{p_0^{(i)}(\boldsymbol{\theta})}{p_0^{(j)}(\boldsymbol{\theta})}=\frac{f_R(r^i)}{f_R(r^j)}=\frac{f_R(\alpha DT)}{f_R(\alpha DT)}=1 \tag{22}$$

Further, since they are all basic Monte Carlo samples selected randomly and evenly based on the amplified excitation, similarly one has

$$\frac{\widetilde{p}^{(i)}(\boldsymbol{\theta})}{\widetilde{p}^{(j)}(\boldsymbol{\theta})}=1 \tag{23}$$

Therefore,

$$\frac{p_0^{(i)}(\boldsymbol{\theta})}{\widetilde{p}^{(i)}(\boldsymbol{\theta})}=\frac{p_0^{(j)}(\boldsymbol{\theta})}{\widetilde{p}^{(j)}(\boldsymbol{\theta})} \tag{24}$$

And the importance ratio $p_0^{(q)}(\boldsymbol{\theta})/\widetilde{p}^{(q)}(\boldsymbol{\theta})$ can be taken as 1 for all these amplified samples in the tail region.

This leads to the following conclusion: in the general cases, using samples from the amplified system for the estimation of the peak of IDC is not feasible. However, it is reasonable to use the amplified samples that fall in the tail region for the tail estimation of the IDC.

3.3. Proposed scheme

Based on the above discussion, to ensure accurate estimation of intrinsic drift coefficients in both peak and tail regions, the following strategy is suggested. The main idea is to use samples from the original system for estimation in the peak range, while supplementing them with samples from the amplified system for estimation in the tail range. In more detail, the procedures can be summarized as the following four steps.

1) Obtain N_0 samples from the original system. The accuracy in the peak range is completely determined by the N_0 samples.
2) Acquire N_a samples from the amplified system with the excitation intensity amplified by factor α. At this stage, $N_a=N_0$ is taken for all examples, and the selection of excitation amplification factors relies on preliminary tests using 50 samples each from the original and amplified systems. An initial amplification factor (e.g. 2) is tested, aiming for 20%–40% of amplified samples in the effective tail range, and adjusted as needed.
3) At each time step, apply a weighting function $w^{(i)}$, $i=1,2,\cdots,N_a$ to the second set of samples.
4) Combine the N_0 samples from the original system with the N_a weighted samples from the amplified system, and numerically estimate the intrinsic drift coefficients. Herein LoWeSS [57] is suggested for the numerical estimation.

The weighting function $w^{(i)}$ is

$$w^{(i)}=\mathscr{H}\left(\frac{\|\widetilde{\boldsymbol{y}}^{(i)}-\overline{\boldsymbol{y}}\|}{\max\limits_{k=1,2,\cdots,N_0}\|\boldsymbol{y}^{(k)}-\overline{\boldsymbol{y}}\|}-\rho\right) \tag{25}$$

where $\mathscr{H}(\cdot)$ denotes the Heaviside function; $\widetilde{\boldsymbol{y}}^{(i)}$ denotes the $i-$th sample value of the dimensions of interests from the amplified system; $\boldsymbol{y}^{(k)}$ denotes the $k-$th sample value of the dimensions of interests from the original system; $\overline{\boldsymbol{y}}$ denotes the mean value of the samples from the original system; $\|\cdot\|$ is the symbol of Euclidean norm; and ρ is a constant value. A schematic figure of the weight function is shown in Fig. 2. For the numerical examples in this work, ρ is taken as 1. Notice that because of the sparsity of samples in the tail region, according to the numerical tests of the authors, a variation between 1 and 1.1 of ρ has almost no impact on the final results.

A flow chart of the proposed procedure is shown in Fig. 3. In the following section, the validity of the proposed scheme will be demonstrated by numerical examples.

4. Numerical examples

4.1. 20-Dimensional Ornstein–Uhlenbeck process

To illustrate the analytical consistency of the IDC before and after

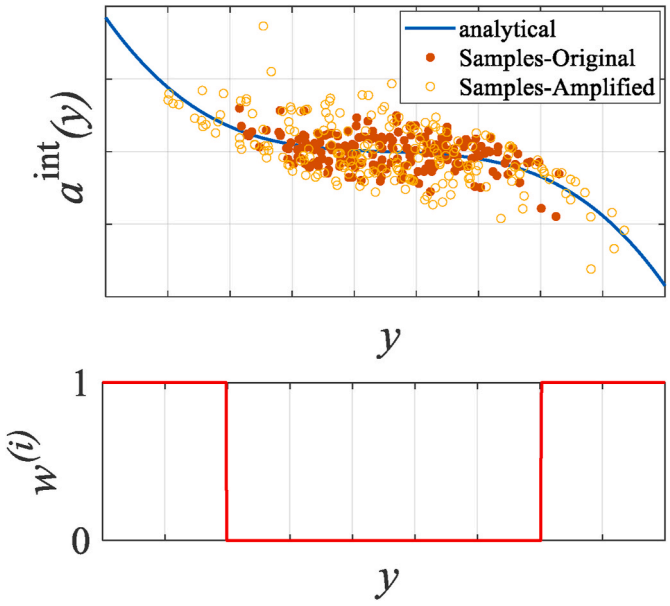

Fig. 2. Schematic of the weighting function $w^{(i)}$ in the proposed scheme.

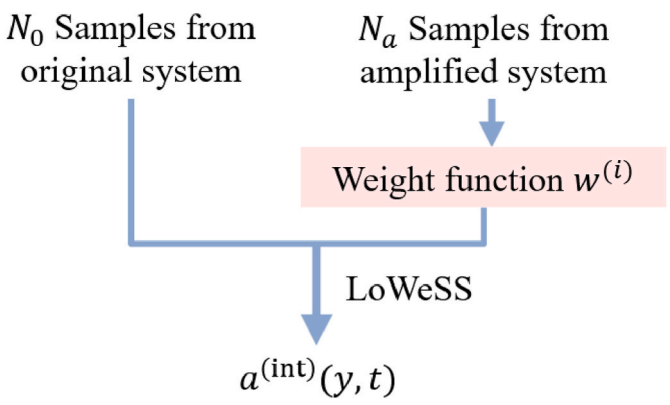

Fig. 3. Flow chart of the proposed scheme.

amplifying the excitation for linear systems, a 20-dimensional Ornstein–Uhlenbeck process is investigated, where the state equation can be given as

$$\dot{\boldsymbol{X}}(t) = \mathbf{K}\boldsymbol{X}(t) + \boldsymbol{b}\xi(t) \tag{26}$$

where $\mathbf{K}$ is a 20×20 matrix given by

$$\mathbf{K} = \begin{bmatrix} -0.2 & 0.04 & & \\ 0.04 & -0.2 & \ddots & \\ & \ddots & \ddots & 0.04 \\ & & 0.04 & -0.2 \end{bmatrix} \tag{27}$$

$\boldsymbol{b}$ is a 20×1 vector given by $\boldsymbol{b} = [1, \cdots, 1]^{\mathrm{T}}$, and $\xi(t)$ is a stationary Gaussian white noise with intensity $\mathrm{E}[\xi(t)\xi(t+\tau)] = D\delta(\tau)$. The original excitation intensity is taken as $D = 0.2$. As comparison, two amplified excitation intensities, i.e. $D = 0.4$, and $D = 0.8$, are considered for the estimation of the IDC for the data-assisted DR-PDEE. The last dimension is the dimension of interest, i.e. $Y = X_{20}$.

For the DR-PDEE scheme, 200 samples are used for the estimation of IDC. In the deterministic analysis of systems with different input intensities, the excitations vary only in the excitation intensity. That means, the input samples of the excitations are proportional. It is already known that, for the current example, the IDC is linear. That is,

$$a^{(\text{int})}(y,t) = k^{(\text{int})}(t) \cdot y \tag{28}$$

Therefore, linear least squares regression is employed for the numerical estimation of IDC. As shown in Fig. 4, the numerically estimated IDCs from samples corresponding to different input intensities are exactly the same. They are all in good agreement with the analytical solution given in Ref. [59]. This is consistent with the previous conclusion that for linear systems with no random parameters involved, the IDCs for different excitation intensities are the same.

Fig. 5 shows the results of the comparison of PDFs at $t = 10$ solved from the DR-PDEE with these numerically estimated IDCs, and the analytical solution. Since the estimated IDCs are exactly the same, the corresponding PDF solutions are identical. They are all in very good agreement with the analytical PDF solution, with only a slight difference in the extreme tail.

4.2. Two-dimensional system with analytical solution

To better showcase the effects of the proposed scheme, a specifically selected single-degree-of-freedom (SDOF) nonlinear system, which is a two-dimensional (2D) system in state space, is first studied. This system is reduced to a one-dimensional (1D) system, whose steady state intrinsic drift coefficient is analytically known and nonlinear. Its equation of motion can be given by

$$\begin{cases} \dot{X}(t) = V(t) \\ \dot{V}(t) = -c\left(\frac{1}{2}V(t)^2 + \frac{k}{2}X(t)^2\right)V(t) - kX(t) + \xi(t) \end{cases} \tag{29}$$

where c and k are constants, and $\xi(t)$ is the Gaussian white noise excitation with intensity $\mathrm{E}[\xi(t)\xi(t+\tau)] = D_0\delta(\tau)$. The steady state analytical solution of the response PDF is given as [62]

$$p_{\mathrm{S}}(x,v) = C_1 \exp\left[-\frac{c}{4D_0}\left(v^4 + 2kx^2v^2 + k^2x^4\right)\right] \tag{30}$$

where C_1 is a normalization constant. If reduce the system into 1D with respect to V, the analytical steady state solution of intrinsic drift coefficients can be given as

$$a_{\mathrm{S}}^{(\text{int})}(v) = \frac{\int\left(-c\left(\frac{1}{2}v^2 + \frac{k}{2}x^2\right)v + kx\right)p_s(x,v)\mathrm{d}x}{\int p_s(x,v)\mathrm{d}x} \tag{31}$$

From Eq. (31) it can be seen that the steady-state analytical IDC is dependent on the white noise intensity.

In this example, the following parameters are selected: $k = 0.02, c = 0.02,$ and $D_0 = 1$. For the tail-enhanced DR-PDEE, the amplified excitation intensity is taken as $\widetilde{D} = 4$. A comparison of the analytical steady-state IDC of the original system with $D_0 = 1$ and the amplified system with $\widetilde{D} = 4$ is given in Fig. 6. As evident, these two IDCs are not identical, although they are very close to each other. By substituting these two analytical IDCs into the DR-PDEE and solving it, the obtained PDF results are compared with the steady-state analytical solution, as depicted in Fig. 4. Using the IDC from the amplified system leads to incorrect results, but the distinction in the PDF tail is almost negligible compared to the apparent error in the peak range. Conversely, the DR-PDEE solution using the analytical IDC from the original system is almost completely consistent with the analytical solution, even in the extreme tail. This suggests that the numerical error in solving the DR-PDEE is negligible (see Fig. 7).

After verifying the DR-PDEE using the analytical IDC, the data-assisted DR-PDEE schemes are studied. The proposed tail-enhanced DR-PDEE solution is obtained, and compared with the classical DR-PDEE solution and the analytical solution. For classical DR-PDEE, 1000 samples are used, and for the proposed tail-enhanced DR-PDEE scheme, 500 samples from the original system together with 500 samples from the amplified system are used for each simulation.

In order to assess the robustness of the proposed method, 20 repeated

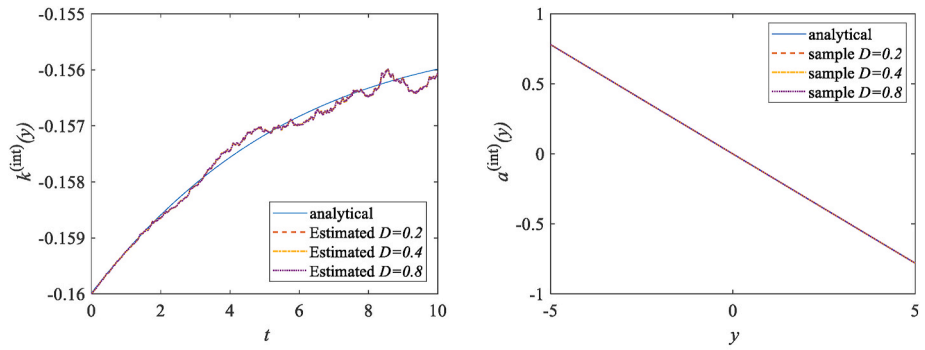

(a) $k^{(\mathrm{int})}(t)$ (b) $a^{(\mathrm{int})}(y)$ at $t=10$

Fig. 4. Comparison of IDCs estimated by samples from different input intensity and the analytical solution.

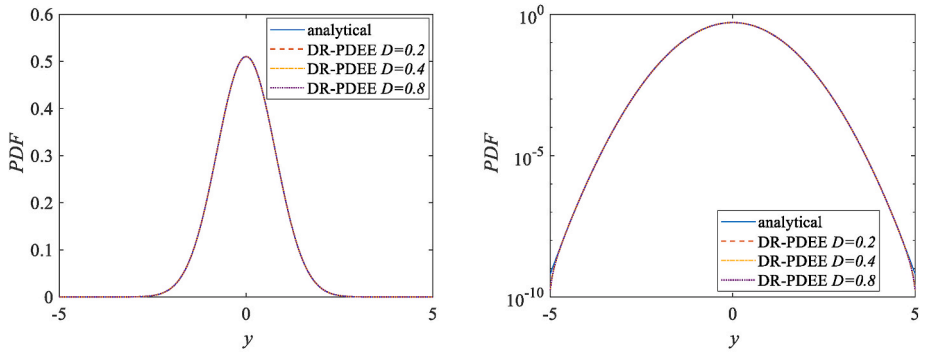

(a) linear scale (b) logarithmic scale

Fig. 5. Comparison of the PDF solutions at $t = 10$ via DR-PDEE using IDCs from various excitation intensity and the analytical solution.

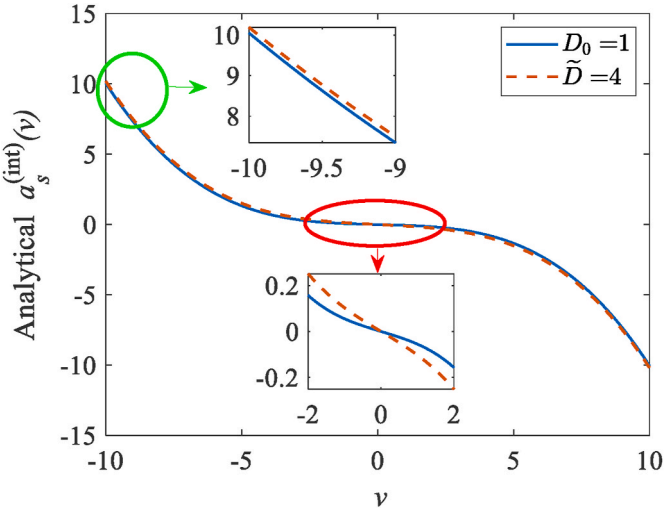

Fig. 6. Comparison of the analytical steady-state IDCs $a_s^{(\mathrm{int})}(v)$ of the original system with $D_0 = 1$ and the amplified system with $\tilde{D} = 4$

simulations are conducted for each DR-PDEE scheme. The obtained mean estimation results and the boundaries are compared with corresponding analytical solution. Figs. 8 and 9 show the results of the intrinsic drift coefficients and the PDF results respectively. Herein, the boundaries in these figures are the maximum and minimum values obtained from the 20 trials of simulation.

It can be seen that though the classical DR-PDEE already has considerable accuracy, the proposed tail-enhanced DR-PDEE shows much higher accuracy and reduced variability in the tail. However, in the peak range, the variation of the solutions obtained by the tail-enhanced DR-PDEE is slightly larger than that of the classical DR-PDEE. This can be easily understood, as when the total number of the samples is identical for the two schemes, fewer samples fall in the peak range for the proposed scheme. In practical application of the tail-enhanced DR-PDEE scheme, it is important to carefully determine the allocation of the sample sizes for the two groups, to ensure a balance between peak and tail accuracy.

4.3. Two-DOF vibro-impact oscillator

Further, consider a two-DOF vibro-impact oscillator subject to Gaussian white noise. Its equation of motion is given by

$$\begin{cases} m_1\ddot{X}_1(t) + c_1\dot{X}_1(t) + k_1X_1(t) + k_2[X_1(t) - X_2(t)] = \xi_1(t) \\ m_2\ddot{X}_2(t) + c_2\dot{X}_2(t) + k_2[X_2(t) - X_1(t)] + F_2[X_2(t)] = \xi_2(t) \end{cases} \tag{32}$$

where $m_1 = m_2 = 1$, $c_1 = 0.4$, $c_2 = 0.2$, $k_1 = k_2 = 0.5$, and $F_2[X_2(t)]$ denotes the impact force from a two-sided barrier. That is,

$$F_2(x_2) = \begin{cases} -B_L(-x_2 - \delta_L)^{3/2}, x_2 \le -\delta_L \\ 0, -\delta_L < x_2 < \delta_R \\ B_R(x_2 - \delta_R)^{3/2}, x_2 \ge \delta_R \end{cases} \tag{33}$$

in which $B_L = B_R = 100$, and $\delta_L = \delta_R = 0.5$. In Eq. (32), ξ_1 and ξ_2 are Gaussian white noises with intensity $D_1 = 0.01$ and $D_2 = 0.005$ respectively. The steady-state joint PDF of $[\boldsymbol{x}, \boldsymbol{v}] = [x_1, v_1, x_2, v_2]$ can be given by

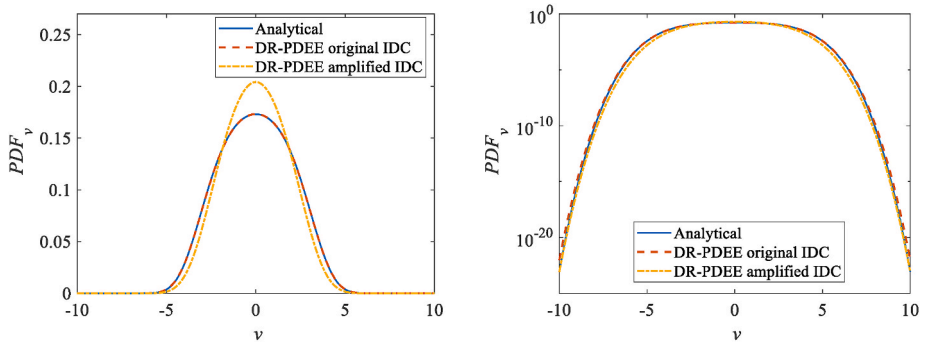

Fig. 7. Comparison of the steady state PDFs of V via DR-PDEE using the analytical steady-state IDCs respectively from original system and amplified system, and analytical solution.

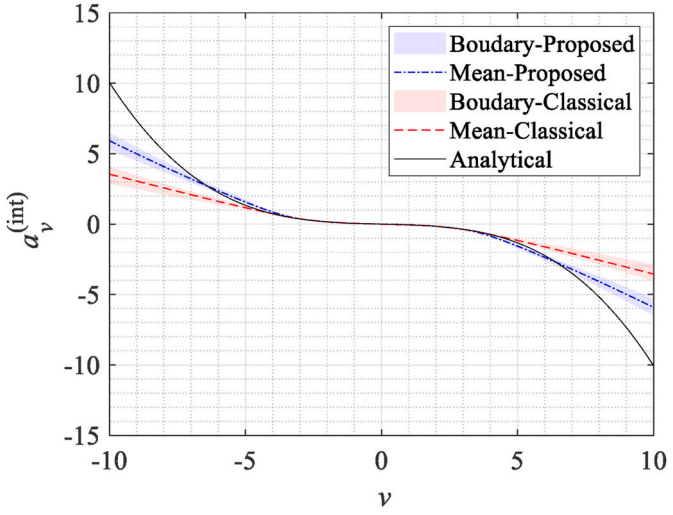

Fig. 8. Comparison of the steady state intrinsic drift coefficients via classical DR-PDEE, proposed tail-enhanced DR-PDEE and analytical solution.

$$p_s(\boldsymbol{x},\boldsymbol{v}) = C_0 \exp\left\{ -2\gamma\left[\frac{m_1 v_1^2}{2}+\frac{m_2 v_2^2}{2}+\frac{k_1 x_1^2}{2}+\frac{k_2(x_1-x_2)^2}{2}+G_2(x_2)\right]\right\} \tag{34}$$

where

$$G_2(x_2) = \begin{cases} \frac{2}{5}B_L(-x_2-\delta_L)^{5/2}, x_2 \le -\delta_L \\ 0, -\delta_L < x_2 < \delta_R \\ \frac{2}{5}B_R(x_2-\delta_R)^{5/2}, x_2 \ge \delta_R \end{cases} \tag{35}$$

The displacement and velocity of the second DOF are considered in this example. The DR-PDEE of the joint PDF of $[X_2, V_2]$ can be cast as

$$\frac{\partial p_{X_2V_2}(x_2,v_2,t)}{\partial t} = -\frac{\partial\left[v_2 p_{X_2V_2}(x_2,v_2,t)\right]}{\partial x_2} - \frac{\partial\left[a_{V_2}^{(\mathrm{int})}(x_2,v_2,t)p_{X_2V_2}(x_2,v_2,t)\right]}{\partial v_2} + \frac{D_2}{2}\frac{\partial^2 p_{X_2V_2}(x_2,v_2,t)}{\partial v_2^2} \tag{36}$$

where the analytical steady state solution of the intrinsic drift coefficients can be derived as [53].

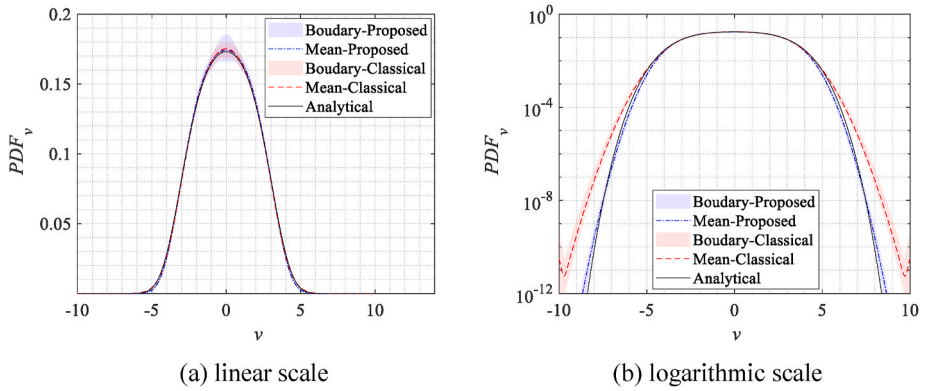

Fig. 9. Comparison of the steady state PDFs of V via classical DR-PDEE, proposed tail-enhanced DR-PDEE and analytical solution.

$$a_{V_2,\mathrm{S}}^{(\mathrm{int})}(x_2,v_2)=\frac{1}{m_2}\left[-c_2v_2-\frac{1}{1/k_1+1/k_2}x_2-F_2(x_2)\right] \tag{37}$$

It can be seen from Eq. (37) that for this nonlinear case, $a_{V_2,\mathrm{S}}^{(\mathrm{int})}(x_2,v_2)$ is independent of the white noise intensity. Further, since the system is energy-equipartitioned [53], and the nonlinearity is only on the displacement term, the intrinsic drift coefficients are set as $\widetilde{a}_{V_2}^{(\mathrm{int})}(x_2,v_2,t)=-\frac{c_2}{m_2}v_2+g(x_2,t)$ in the following data-based estimation.

In both the classical and proposed tail-enhanced DR-PDEE scheme, 400 samples are used for the estimation. Specifically, for the proposed scheme, 200 samples from the amplified system and 200 samples from the original system are employed, where the amplified excitation intensity is taken as $\widetilde{D}_2=9D_2$. 20 repeated simulations are conducted for the classical and proposed DR-PDEE scheme. The mean solutions, as well as the maximum and minimum boundaries of the 20 simulations are obtained.

Figs. 10 and 11 depict the time-varying solution of the standard deviation and kurtosis of X_2 and V_2 obtained from the classical DR-PDEE and the proposed tail-enhanced DR-PDEE respectively. The results are also compared with the corresponding analytical steady-state solutions. It can be seen that both of the classical and tail-enhanced DR-PDEE well capture the second and fourth order moments of the responses, while the proposed scheme yields slightly better results for the kurtosis estimation.

Figs. 12 and 13 show the steady-state PDF results of X_2 and V_2. Similar to the previous example, compared with the classical DR-PDEE, the tail-enhanced DR-PDEE exhibits much higher accuracy and smaller variation in the tail range, while showing slightly larger variation in the peak range.

4.4. 10-DOF Duffing Oscillator with random parameters

Consider a 10-DOF Duffing oscillator with random stiffness. Its equation of motion is given by

$$\mathbf{M}\ddot{\boldsymbol{X}}(t)+\mathbf{C}\dot{\boldsymbol{X}}(t)+\boldsymbol{f}[\boldsymbol{X}(t),\boldsymbol{\Theta}]=\boldsymbol{B}\xi(t) \tag{38}$$

In this equation, $\boldsymbol{X}(t)$, $\dot{\boldsymbol{X}}(t)$, and $\ddot{\boldsymbol{X}}(t)$ respectively denote the displacement, velocity, and acceleration. $\mathbf{M}=\mathrm{diag}[3,3,3,3,2,2,2,2,1.5,1.5]\times10^5$ is the diagonal mass matrix. $\mathbf{C}=a_0\mathbf{M}+a_1\mathbf{K}(\boldsymbol{\Theta})$ is the linear damping matrix dependent on the random stiffness matrix, where

$$\mathbf{K}(\boldsymbol{\Theta})=\begin{bmatrix}\theta_1k_1+\theta_2k_2 & -\theta_2k_2 & & & & \\ -\theta_2k_2 & \theta_2k_2+\theta_3k_3 & -\theta_3k_3 & & & \\ & \ddots & \ddots & \ddots & & \\ & & -\theta_9k_9 & \theta_9k_9+\theta_{10}k_{10} & -\theta_{10}k_{10} \\ & & & -\theta_{10}k_{10} & \theta_{10}k_{10}\end{bmatrix} \tag{39}$$

$$\begin{pmatrix}a_0\\ a_1\end{pmatrix}=\frac{2\zeta}{\omega_1+\omega_3}\begin{Bmatrix}\omega_1\omega_3\\ 1\end{Bmatrix} \tag{40}$$

$[k_1,k_2,\cdots,k_{10}]=[5,5,5,5,4,4,4,4,3,3]\times10^7$, $[\theta_1,\theta_2,\cdots,\theta_{10}]$ are 10 independent identically distributed log-normal random variables with unit mean and coefficient of variation equal to 0.15, ω_1 and ω_3 are respectively the square root of the first and third minimum eigenvalue of $\mathbf{M}^{-1}\mathbf{K}(\boldsymbol{\Theta})$, and $\zeta=0.05$ is the damping ratio. The restoring force is

$$\boldsymbol{f}[\boldsymbol{X}(t)]=\left[f_1^*-f_2^*,f_2^*-f_3^*,\cdots,f_{n-1}^*-f_n^*,f_n^*\right] \tag{41}$$

where

$$f_j^*=k_j\left[\widehat{X}_j+\frac{\varepsilon}{\sigma_s^2}\widehat{X}_j^3\right],\ \text{for}\ j=1,\cdots,n \tag{42}$$

$\widehat{X}_j$ is the $j-$th element of the inter-story drift vector $\widehat{\boldsymbol{X}}=[X_1,X_2-X_1,\cdots,X_n-X_{n-1}]^T$, ε is a dimensionless constant, and σ_s^2 is the steady-state variance of X_1 for the corresponding linear system by setting $\varepsilon=0$. $\xi(t)$ is a one-dimensional stationary Gaussian white noise with correlation function $R_\xi(\tau)=D_0\delta(\tau)$, $D_0=0.2$, and $\boldsymbol{B}=[1,1,\cdots,1]^{\mathrm{T}}$. In this case, $\sigma_s^2=0.0036$ is obtained from Monte Carlo simulation (MCS) with 10^4 samples. $\varepsilon=0.72$ is taken, and therefore $\frac{\varepsilon}{\sigma_s^2}=200$.

Assume the displacement of the first DOF $X_1(t)$ is the quantity of interest. Since there is no excitation term in that dimension, the velocity of the first DOF $V_1(t)$ is introduced to construct a two-dimensional system for the DR-PDEE analysis. For the proposed scheme, the amplified excitation intensity is taken as $\widetilde{D}=0.4$. Similarly, 20 repeated simulations are conducted for the classical and proposed DR-PDEE scheme. For classical DR-PDEE method, 400 samples are used, and for the proposed tail-enhanced DR-PDEE scheme, 200 samples from the original system and 200 samples from the amplified system are used for each simulation. The obtained results are compared with MCS with 10^6 samples for verification.

The time-varying standard deviation and kurtosis of $X_1(t)$ are shown in Fig. 14, where the boundaries are defined as

$$b_\pm=\mu(f)\pm\sigma(f) \tag{43}$$

where f denotes the function of concern, $\mu(\cdot)$ denotes the mean value, and $\sigma(\cdot)$ denotes the standard deviation. Fig. 15 shows the comparison of the steady state PDFs and CDFs of $X_1(t)$. To avoid negative values, the boundaries are defined as

$$b_\pm=\exp\{\mu[\ln(f)]\pm\sigma[\ln(f)]\} \tag{44}$$

Both of the classical and proposed tail-enhanced DR-PDEE scheme obtain good estimation with respect to the time-varying standard deviation and kurtosis. Better results are obtained in the CDF tail when using the proposed scheme, though the improvement is not as prominent as the previous two examples, since the classical DR-PDEE already has considerable tail accuracy.

5. Concluding remarks

An easy-to-implement scheme has been proposed to enhance the tail accuracy of the dimension-reduced probability density evolution equation (DR-PDEE) method for stochastic dynamic response analysis of complex multi-dimensional nonlinear systems. The key idea is to obtain samples in the tail range by amplifying the excitation intensity. These samples are then weighted and combined with samples from the original system for a better estimation of the intrinsic drift coefficients in the DR-

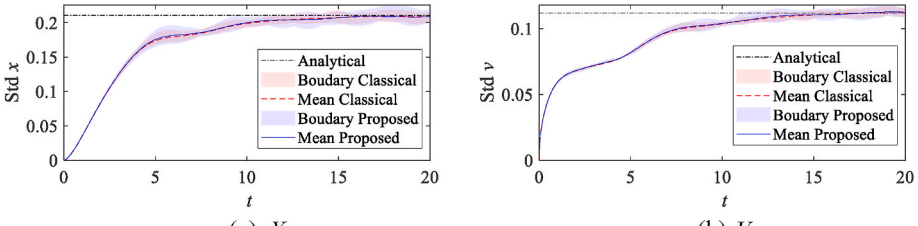

(a) X_2 (b) V_2

Fig. 10. Comparison of the analytical steady-state standard deviation and time-varying solutions via classical DR-PDEE and proposed tail-enhanced DR-PDEE.

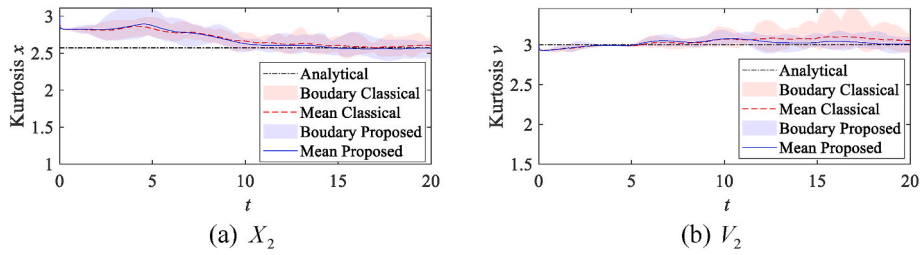

Fig. 11. Comparison of the analytical steady-state kurtosis and time-varying solutions via classical DR-PDEE and proposed tail-enhanced DR-PDEE.

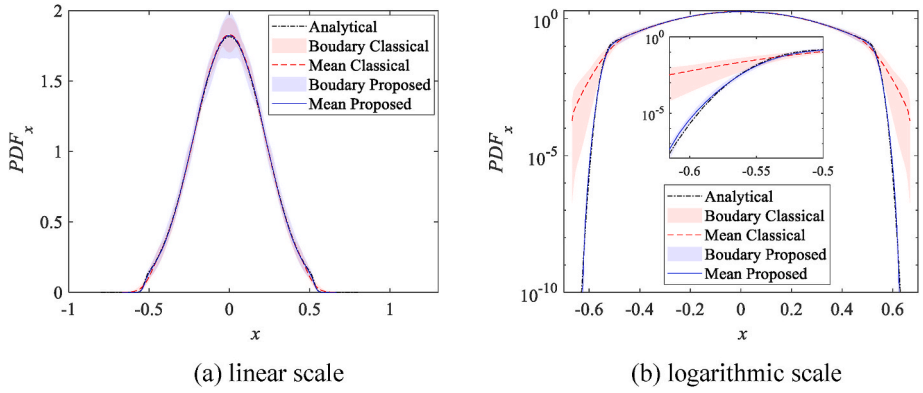

Fig. 12. Comparison of the steady state PDFs of X_2 via classical DR-PDEE, proposed tail-enhanced DR-PDEE and the analytical solution.

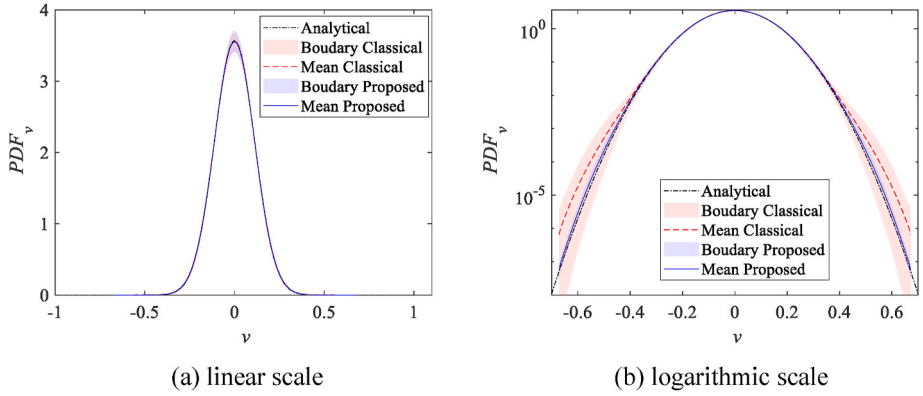

Fig. 13. Comparison of the steady state PDFs of V_2 via classical DR-PDEE, proposed tail-enhanced DR-PDEE and the analytical solution.

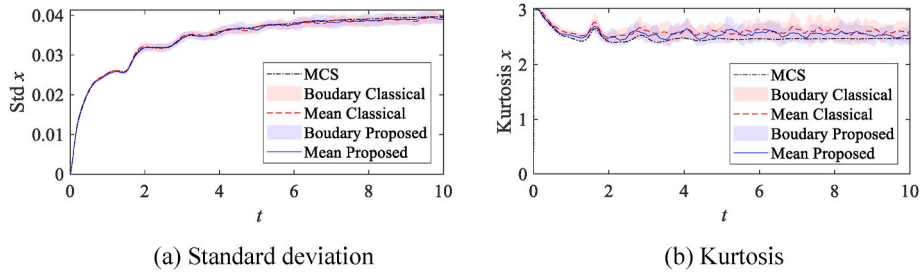

Fig. 14. Comparison of the standard deviation and kurtosis of $X_1(t)$ via classical DR-PDEE, proposed tail-enhanced DR-PDEE and MCS.

PDEE. The tail accuracy of the DR-PDEE method has been significantly improved, as illustrated by several numerical examples.

Although the rationality of the proposed scheme has been elucidated from an importance sampling point of view, a more rigorous proof from the perspective of system physics is still desired. Though several linear and nonlinear systems have been studied, more investigations, such as hysteretic systems, still need to be conducted.

Further, in the practical application of the proposed tail-enhanced DR-PDEE scheme, the selection of the excitation amplifying factor and the number of excitation-amplified samples can be flexible and optimized. It is possible to combine the samples from various excitation-amplified systems with different excitation amplifying factors. To achieve the balance between the peak and tail accuracy, optimization schemes can be developed and employed for the allocation of samples,

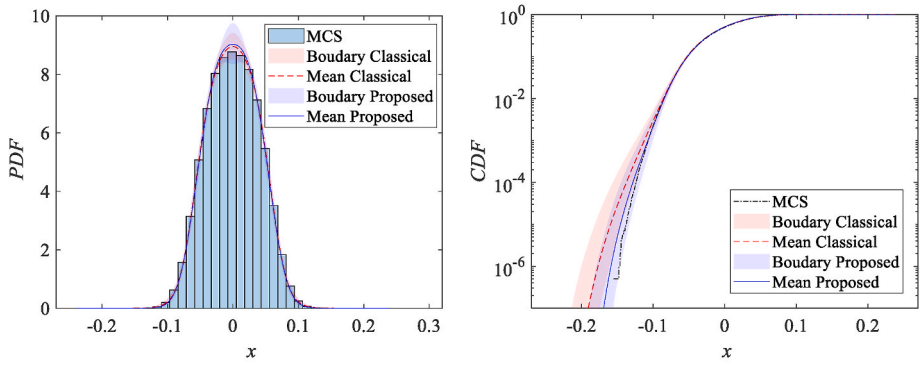

(a) PDF (linear scale) (b) CDF (logarithmic scale)

Fig. 15. Comparison of the steady state PDFs and CDFs of $X_1(t)$ via classical DR-PDEE, proposed tail-enhanced DR-PDEE and MCS.

which is beyond the scope of the current contribution and needs to be further investigated.

Finally, the proposed method is expected to further improve the accuracy of the DR-PDEE method in the reliability and extreme value analysis of complex nonlinear systems.

CRediT authorship contribution statement

Yi Luo: Writing – review & editing, Writing – original draft, Visualization, Validation, Software, Methodology, Investigation, Formal analysis, Conceptualization. **Chao Dang:** Writing – review & editing, Methodology, Conceptualization. **Matteo Broggi:** Writing – review & editing, Supervision, Project administration, Funding acquisition. **Michael Beer:** Writing – review & editing, Supervision, Project administration, Funding acquisition.

Declaration of competing interest

The authors declare that they have no known competing financial interests or personal relationships that could have appeared to influence the work reported in this paper.

Acknowledgement

The authors are grateful for the support by the European Union's Horizon 2020 research and innovation programme under Marie Sklodowska-Curie project GREYDIENT – Grant Agreement n∘955393. We sincerely acknowledge Prof. Pol D. Spanos from Rice University for his invaluable suggestions on the theoretical refinement of this work. We also extend our deep gratitude to Ms. Tingting Sun from Tongji University for her generous assistance with the analytical solutions for energy-equipartition systems in the appendix. Additionally, we are profoundly thankful to Dr. Meng-Ze Lyu and Prof. Jian-bing Chen from Tongji University for their insightful comments to this work.

Appendix. A special category of nonlinear systems with IDC independent of excitation intensity

Consider an $n-$ DOF dynamic system given by

$$\mathbf{M}\ddot{\boldsymbol{X}}(t)+\mathbf{C}\dot{\boldsymbol{X}}(t)+\boldsymbol{f}[\boldsymbol{X}(t)]=\boldsymbol{\xi}(t) \tag{45}$$

In this equation, $\mathbf{M}$ is a diagonal mass matrix. $\mathbf{C}$ is a diagonal damping matrix which satisfies $\mathbf{C}=\gamma\boldsymbol{D}$, where $\gamma>0$ is a constant. $\boldsymbol{D}$ is the diagonal intensity matrix of the Gaussian white noise excitation $\boldsymbol{\xi}(t)$. That is, $\mathrm{E}[\boldsymbol{\xi}(t)]=0$, and $\mathrm{E}[\boldsymbol{\xi}(t)\boldsymbol{\xi}(t+\tau)]=\boldsymbol{D}\delta(\tau)$. The restoring force $\boldsymbol{f}[\boldsymbol{X}(t)]$ satisfies

$$f_i(\boldsymbol{X})=\frac{\partial U(\boldsymbol{X})}{\partial X_i} \tag{46}$$

where $U(\boldsymbol{X})$ is the potential of the system. With all these assumptions, the system is an energy equipartition system [11,53].

Further, consider $X_l(t)$ and $V_l(t)$ as the response quantity of interest. If the potential $U(\boldsymbol{X})$ of the system can be transferred into

$$U(\boldsymbol{X})=g_1(X_l)+g_2(\boldsymbol{Y}) \tag{47}$$

where $\boldsymbol{Y}=\boldsymbol{h}(\boldsymbol{X})$ is a multi-dimension function with respect to the system response, and each component of $\boldsymbol{Y}$ are all independent of X_l. $g_1(\cdot)$ and $g_2(\cdot)$ are deterministic function irrelevant with the excitation intensity. Then the steady-state intrinsic drift coefficient (IDC) with respect to $X_l(t)$ and $V_l(t)$ can be given as

$$\boldsymbol{a}_s^{(\mathrm{int})}(x_l,v_l)=\begin{bmatrix} v_l \\ -\dfrac{c_l}{m_l}v_l-\dfrac{1}{m_l}\dfrac{\partial g_1(x_l)}{\partial x_l} \end{bmatrix} \tag{48}$$

which is independent with the intensity of the excitation. Thus, varying the excitation intensity will not change the IDC in the DR-PDEE.

This can be easily proven. The second term of $\boldsymbol{a}_s^{(\mathrm{int})}(x_l,v_l)$ can be derived as

$$
\begin{aligned}
&\boldsymbol{a}_{s,2}^{(\mathrm{int})}(x_l, v_l) \\
&= -\frac{1}{m_l}\mathrm{E}[c_l V_l + F_l(\boldsymbol{X})|X_l = x_l, V_l = v_l] \\
&= -\frac{1}{m_l}c_l v_l - \frac{1}{m_l}\mathrm{E}\left[\frac{\partial U(\boldsymbol{X})}{\partial X_l}\middle| X_l = x_l\right] \\
&= -\frac{1}{m_l}c_l v_l - \frac{1}{m_l}\mathrm{E}\left[\frac{\partial U(X_l, \boldsymbol{Y})}{\partial X_l}\middle| X_l = x_l\right] \\
&= -\frac{1}{m_l}c_l v_l - \frac{1}{m_l}\frac{\partial g_1(x_l)}{\partial x_l}.
\end{aligned} \tag{49}
$$

An easy-to-illustrate example of this type of system is the MDOF tandem Duffing Oscillator in Sun and Chen [53]. In this system, the potential energy is

$$
U(\boldsymbol{x}) = \frac{1}{2}k_1 x_1^2 + \frac{1}{4}\alpha_1 k_1 x_1^4 + \sum_{i=2}^{n}\left[\frac{1}{2}k_i(x_i - x_{i-1})^2 + \frac{1}{4}\alpha_i k_i (x_i - x_{i-1})^4\right] \tag{50}
$$

where k_i and α_i ($i = 1, \cdots, n$) are system parameter with respect to the restoring fore. Note that the steady state response PDF of an energy equipartition system can be given as [9,63]

$$
p_{\boldsymbol{X},\boldsymbol{V},s}(\boldsymbol{x}, \boldsymbol{v}) = C_0 \exp[-2\gamma H(\boldsymbol{x}, \boldsymbol{v})] \tag{51}
$$

where C_0 is a normalization constant, $H(\boldsymbol{x}, \boldsymbol{v}) = T(\boldsymbol{v}) + U(\boldsymbol{x})$ denotes the Hamiltonian, i.e. the sum of the kinetic energy $T(\boldsymbol{v})$ and potential energy $U(\boldsymbol{x})$, and

$$
T(\boldsymbol{v}) = \sum_{i=1}^{n}\frac{1}{2}m_i V_i^2 \tag{52}
$$

Substituting the potential energy in Eq. (50) into Eq. (51), it can be readily found that the relative displacements of each dimension $X_1, X_2 - X_1, \cdots, X_n - X_{n-1}$, and the absolute velocities of each dimension $V_1, V_2, \cdots, V_n$ are independent. In this case, suppose the displacement and velocity of the first DOF are dimensions of interests. Therefore, $X_l = X_1,$ and $\boldsymbol{Y} = [X_2 - X_1, \cdots, X_n - X_{n-1}]^{\mathrm{T}}$. The corresponding intrinsic drift coefficient is [53]

$$
\boldsymbol{a}_s^{(\mathrm{int})}(x_1, v_1) = \begin{bmatrix} v_1 \\ -\dfrac{c_1}{m_1}v_1 - \dfrac{1}{m_l}\left(k_1 x_1 + \alpha_1 k_1 x_1^3\right) \end{bmatrix} \tag{53}
$$

with no excitation-related term involved in this closed-form solution.

Data availability

No data was used for the research described in the article.

References

[1] J.B. Roberts, P.D. Spanos, Random vibration and statistical linearization, Courier Corporation (2003).
[2] J. Li, J. Chen, Stochastic Dynamics of Structures, John Wiley & Sons, 2009 Jul 23.
[3] N.C. Nigam, S. Narayanan, Applications of Random Vibrations, Narosa Publishing House, 1994 Jan.
[4] W.K. Liu, A. Mani, T. Belytschko, Finite element methods in probabilistic mechanics, Probabilist. Eng. Mech. 2 (4) (1987 Dec 1) 201–213.
[5] D. Xiu, J.S. Hesthaven, High-order collocation methods for differential equations with random inputs, SIAM J. Sci. Comput. 27 (3) (2005) 1118–1139.
[6] M.M. Dannert, F. Bensel, A. Fau, R.M. Fleury, U. Nackenhorst, Investigations on the restrictions of stochastic collocation methods for high dimensional and nonlinear engineering applications, Probabilist. Eng. Mech. 69 (2022 Jul 1) 103299.
[7] R.G. Ghanem, P.D. Spanos, Stochastic finite elements: a spectral approach, Courier Corporation (2003).
[8] C.W. Gardiner, Handbook of Stochastic Methods, 3rd-Edn., Springer-Verlag, Berlin Heidelberg, 2004.
[9] W.Q. Zhu, G.Q. Cai, Y.K. Lin, On exact stationary solutions of stochastically perturbed Hamiltonian systems, Probabilist. Eng. Mech. 5 (2) (1990 Jun 1) 84–87.
[10] C. Soize, The Fokker-Planck equation for stochastic dynamical systems and its explicit steady state solutions, World Scientific (1994).
[11] W.Q. Zhu, Z.L. Huang, Exact stationary solutions of stochastically excited and dissipated partially integrable Hamiltonian systems, Int. J. Non Lin. Mech. 36 (1) (2001 Jan 1) 39–48.
[12] B.F. Spencer, L.A. Bergman, On the numerical solution of the Fokker-Planck equation for nonlinear stochastic systems, Nonlinear Dynam. 4 (1993 Aug) 357–372.
[13] J.S. Chang, G. Cooper, A practical difference scheme for Fokker-Planck equations, J. Comput. Phys. 6 (1) (1970 Aug 1) 1–6.
[14] A. Naess, B.K. Hegstad, Response statistics of van der Pol oscillators excited by white noise, Nonlinear Dynam. 5 (1994 Apr) 287–297.
[15] J.B. Roberts, P.D. Spanos, Stochastic averaging: an approximate method of solving random vibration problems, Int. J. Non Lin. Mech. 21 (2) (1986 Jan 1) 111–134.
[16] W.Q. Zhu, Stochastic averaging methods in random vibration, Appl. Mech. Rev. 41 (5) (1988) 189.
[17] G.K. Er, V.P. Iu, State-space-split method for some generalized Fokker-Planck-Kolmogorov equations in high dimensions, Phys. Rev. 85 (6) (2012 Jun 20) 067701.
[18] S.H. Crandall, Non-Gaussian closure for random vibration of non-linear oscillators, Int. J. Non Lin. Mech. 15 (4–5) (1980 Jan 1) 303–313.
[19] H.K. Joo, T.P. Sapsis, A moment-equation-copula-closure method for nonlinear vibrational systems subjected to correlated noise, Probabilist. Eng. Mech. 46 (2016 Oct 1) 120–132.
[20] M.D. McKay, R.J. Beckman, W.J. Conover, A comparison of three methods for selecting values of input variables in the analysis of output from a computer code, Technometrics 42 (1) (2000 Feb 1) 55–61.
[21] M.D. Shields, J. Zhang, The generalization of Latin hypercube sampling, Reliab. Eng. Syst. Saf. 148 (2016 Apr 1) 96–108.
[22] H. Niederreiter, Random Number Generation and Quasi-Monte Carlo Methods, Society for Industrial and Applied Mathematics, 1992 Jan 1.
[23] K.T. Fang, Y. Wang, Number-Theoretic Methods in Statistics, Chapman & Hall, 1994.
[24] X. Zhang, M.D. Pandey, Structural reliability analysis based on the concepts of entropy, fractional moment and dimensional reduction method, Struct. Saf. 43 (2013 Jul 1) 28–40.
[25] J. Xu, C. Dang, A novel fractional moments-based maximum entropy method for high-dimensional reliability analysis, Appl. Math. Model. 75 (2019 Nov 1) 749–768.
[26] G. Li, Y.X. Wang, Y. Zeng, W.X. He, A new maximum entropy method for estimation of multimodal probability density function, Appl. Math. Model. 102 (2022 Feb 1) 137–152.
[27] C. Ding, C. Dang, M.A. Valdebenito, M.G. Faes, M. Broggi, M. Beer, First-passage probability estimation of high-dimensional nonlinear stochastic dynamic systems by a fractional moments-based mixture distribution approach, Mech. Syst. Signal Process. 185 (2023 Feb 15) 109775.
[28] S.K. Au, J.L. Beck, Estimation of small failure probabilities in high dimensions by subset simulation, Probabilist. Eng. Mech. 16 (4) (2001 Oct 1) 263–277.
[29] I. Papaioannou, W. Betz, K. Zwirglmaier, D. Straub, MCMC algorithms for subset simulation, Probabilist. Eng. Mech. 41 (2015 Jul 1) 89–103.

[30] G.I. Schuëller, R. Stix, A critical appraisal of methods to determine failure probabilities, Struct. Saf. 4 (4) (1987 Jan 1) 293–309.
[31] A. Tabandeh, G. Jia, P. Gardoni, A review and assessment of importance sampling methods for reliability analysis, Struct. Saf. 97 (2022 Jul 1) 102216.
[32] P.S. Koutsourelakis, H.J. Pradlwarter, G.I. Schueller, Reliability of structures in high dimensions, part I: algorithms and applications, Probabilist. Eng. Mech. 19 (4) (2004 Oct 1) 409–417.
[33] C. Dang, M.A. Valdebenito, J. Song, P. Wei, M. Beer, Estimation of small failure probabilities by partially Bayesian active learning line sampling: theory and algorithm, Comput. Methods Appl. Mech. Eng. 412 (2023) 116068. Jul 1.
[34] C. Dang, M.A. Valdebenito, M.G. Faes, J. Song, P. Wei, M. Beer, Structural reliability analysis by line sampling: a Bayesian active learning treatment, Struct. Saf. 104 (2023) 102351. Sep. 1.
[35] O. Ditlevsen, R. Olesen, G. Mohr, Solution of a class of load combination problems by directional simulation, Struct. Saf. 4 (2) (1986 Jan 1) 95–109.
[36] J. Nie, B.R. Ellingwood, A new directional simulation method for system reliability. Part I: application of deterministic point sets, Probabilist. Eng. Mech. 19 (4) (2004 Oct 1) 425–436.
[37] J. Chan, I. Papaioannou, D. Straub, An adaptive subset simulation algorithm for system reliability analysis with discontinuous limit states, Reliab. Eng. Syst. Saf. 225 (2022 Sep 1) 108607.
[38] Z. Song, H. Zhang, L. Zhang, Z. Liu, P. Zhu, An estimation variance reduction-guided adaptive Kriging method for efficient time-variant structural reliability analysis, Mech. Syst. Signal Process. 178 (2022 Oct 1) 109322.
[39] C. Song, R. Kawai, Monte Carlo and variance reduction methods for structural reliability analysis: a comprehensive review, Probabilist. Eng. Mech. 19 (2023 Jun) 103479.
[40] G.I. Schuëller, H.J. Pradlwarter, P.S. Koutsourelakis, A critical appraisal of reliability estimation procedures for high dimensions, Probabilist. Eng. Mech. 19 (4) (2004 Oct 1) 463–474.
[41] M.Z. Lyu, J.B. Chen, A unified formalism of the GE-GDEE for generic continuous responses and first-passage reliability analysis of multi-dimensional nonlinear systems subjected to non-white-noise excitations, Struct. Saf. 98 (2022 Sep 1) 102233.
[42] J.B. Chen, M.Z. Lyu, Globally-evolving-based generalized density evolution equation for nonlinear systems involving randomness from both system parameters and excitations, Proceedings of the Royal Society A 478 (2264) (2022 Aug 31) 20220356.
[43] J. Li, J.B. Chen, Probability density evolution method for dynamic response analysis of structures with uncertain parameters, Comput. Mech. 34 (5) (2004 Oct) 400–409.
[44] M.Z. Lyu, D.C. Feng, J.B. Chen, J. Li, A decoupled approach for determination of the joint probability density function of a high-dimensional nonlinear stochastic dynamical system via the probability density evolution method, Comput. Methods Appl. Mech. Eng. 418 (2024 Jan 1) 116443.
[45] J. Chen, S. Yuan, PDEM-based dimension-reduction of FPK equation for additively excited hysteretic nonlinear systems, Probabilist. Eng. Mech. 38 (2014 Oct 1) 111–118.
[46] J. Chen, P. Lin, Dimension-reduction of FPK equation via equivalent drift coefficient, Theoret. Appl. Mecha. Lett. 4 (1) (2014 Jan 1) 013002.
[47] J. Chen, Z. Rui, Dimension-reduced FPK equation for additive white-noise excited nonlinear structures, Probabilist. Eng. Mech. 53 (2018 Jun 1) 1–3.
[48] J. Li, Z. Jiang, A data-based CR-FPK method for nonlinear structural dynamic systems, Theoret. Appl. Mecha. Lett. 8 (4) (2018 Jul 1) 231–244.
[49] Y. Luo, J. Chen, P.D. Spanos, Determination of monopile offshore structure response to stochastic wave loads via analog filter approximation and GV-GDEE procedure, Probabilist. Eng. Mech. 67 (2022) 103197. Jan 1.
[50] Y. Luo, P.D. Spanos, J. Chen, Stochastic response determination of multi-dimensional nonlinear systems endowed with fractional derivative elements by the GE-GDEE, Int. J. Non Lin. Mech. 23 (2022) 104247. Sep.
[51] M.Z. Lyu, J.B. Chen, J.X. Shen, Refined probabilistic response and seismic reliability evaluation of high-rise reinforced concrete structures via physically driven dimension-reduced probability density evolution equation, Acta Mech. 18 (2023 Aug) 1–27.
[52] T. Sun, M. Lyu, J. Chen, Property of intrinsic drift coefficients in globally-evolving-based generalized density evolution equation for the first-passage reliability assessment, Acta Mech. Sin. 39 (4) (2023 Apr) 722471.
[53] T. Sun, J. Chen, Physically driven exact dimension reduction of a class of nonlinear multidimensional systems subjected to additive white noise, ASCE-ASME J. Risk Uncert. Eng. Sys. Part A: Civ. Eng. 8 (2) (2022 Jun 1) 04022012.
[54] H.A. Kramers, Brownian motion in a field of force and the diffusion model of chemical reactions, Physica 7 (4) (1940 Apr 1) 284–304.
[55] J. Moyal, Stochastic processes and statistical physics, J. Roy. Stat. Soc. B 11 (2) (1949 Jan 1) 150–210.
[56] H. Risken, The Fokker-Planck Equation, 2nd-Edn., Springer-Verlag, Berlin Heidelberg, 1989.
[57] W.S. Cleveland, Robust locally weighted regression and smoothing scatterplots, J. Am. Stat. Assoc. 1 (1979 Dec) 829–836.
[58] Y. Luo, M.Z. Lyu, J.B. Chen, P.D. Spanos, Equation governing the probability density evolution of multi-dimensional linear fractional differential systems subject to Gaussian white noise, Theoret. Appl. Mecha. Lett. 13 (3) (2023 May 1) 100436.
[59] M.Z. Lyu, J.B. Chen, First-passage reliability of high-dimensional nonlinear systems under additive excitation by the ensemble-evolving-based generalized density evolution equation, Probabilist. Eng. Mech. 63 (2021 Jan 1) 103119.
[60] Y. Leng, Z.H. Lu, C.H. Cai, C.Q. Li, Y.G. Zhao, Ring simulation: a novel simple and efficient simulation method for structural reliability analysis, Struct. Saf. 96 (2022 May 1) 102182.
[61] L.S. Katafygiotis, K.M. Zuev, Geometric insight into the challenges of solving high-dimensional reliability problems, Probabilist. Eng. Mech. 23 (2–3) (2008 Apr 1) 208–218.
[62] Y. Yong, Y. Lin, Exact stationary-response solution for second order nonlinear systems under parametric and external white-noise excitations, J. Appl. Mech. 54 (2) (1987) 414–418.
[63] T.K. Caughey, Derivation and application of the Fokker-Planck equation to discrete nonlinear dynamic systems subjected to white random excitation, J. Acoust. Soc. Am. 35 (11) (1963 Nov) 1683–1692.